Editors' Suggestion | Featured in Physics

Simple Rules Govern the Patterns of Arctic Sea Ice Melt Ponds

Predrag Popović,[1,*] B. B. Cael,[2] Mary Silber,[3] and Dorian S. Abbot[1]
[1]Department of the Geophysical Sciences, The University of Chicago, Chicago, Illinois 60637, USA
[2]Department of Earth, Atmospheric and Planetary Sciences, Massachusetts Institute of Technology, Cambridge, Massachusetts 02139, USA
[3]Department of Statistics and Committee on Computational and Applied Mathematics, The University of Chicago, Chicago, Illinois 60637, USA

(Received 23 October 2017; published 4 April 2018)

Climate change, amplified in the far north, has led to rapid sea ice decline in recent years. In the summer, melt ponds form on the surface of Arctic sea ice, significantly lowering the ice reflectivity (albedo) and thereby accelerating ice melt. Pond geometry controls the details of this crucial feedback; however, a reliable model of pond geometry does not currently exist. Here we show that a simple model of voids surrounding randomly sized and placed overlapping circles reproduces the essential features of pond patterns. The only two model parameters, characteristic circle radius and coverage fraction, are chosen by comparing, between the model and the aerial photographs of the ponds, two correlation functions which determine the typical pond size and their connectedness. Using these parameters, the void model robustly reproduces the ponds' area-perimeter and area-abundance relationships over more than 6 orders of magnitude. By analyzing the correlation functions of ponds on several dates, we also find that the pond scale and the connectedness are surprisingly constant across different years and ice types. Moreover, we find that ponds resemble percolation clusters near the percolation threshold. These results demonstrate that the geometry and abundance of Arctic melt ponds can be simply described, which can be exploited in future models of Arctic melt ponds that would improve predictions of the response of sea ice to Arctic warming.

DOI: 10.1103/PhysRevLett.120.148701

Arctic sea ice plays a major role in Arctic climate [1], ecology [2], and economy. Sea ice's recent rapid decline is a hallmark of climate change [3] that global climate models have systematically underestimated [4]. This is believed to be largely due to small-scale processes that cannot be captured accurately by large-scale models [5]. One such process is the formation of melt ponds on the ice surface during the summer [6]. Melt ponds absorb significantly more sunlight than the surrounding ice, making ponded ice melt faster, creating a positive feedback [7,8]. The central importance of melt ponds was demonstrated in 2014 by Schröder *et al.* [9] who showed that the September sea ice minimum extent can be accurately predicted solely based on spring melt pond fraction. Current models of melt ponds include comprehensive representations of many physical processes and are capable of reproducing Arctic-scale spatial distributions of pond coverage [10–13]. However, their complexity and numerous assumptions reduce their ability to provide a fundamental understanding of pond evolution, and call into question their applicability in a changing climate.

Ponds typically evolve through several stages that are controlled by ice permeability [14,15]. Early in the season (typically late spring and early summer), ice is impermeable so that melt ponds can exist above sea level and cover a large portion of the ice. Later in the season, as ice permeability increases, the ponds drain to the ocean so that remaining ponds correspond to regions of sea ice that are below sea level. After drainage, ponds have a typical length scale of several meters, likely determined by the scale of winter snow dunes [16], and are often connected by channels that form during drainage. This post-drainage stage is typically the longest part of melt pond evolution. An aerial photograph of drained melt ponds is shown in Fig. 1(a).

Melt pond geometry has been shown to control the strength of lateral melting of ice by pond water [17], to impact the pattern of floe breakup [18], and to set the landscape of available light for the organisms living beneath the ice [19]. Several critical observations have previously been made about pond geometry. Hohenegger *et al.* [20] showed that the fractal dimension, D, of late-summer melt ponds, which characterizes their area-perimeter relationship ($P \propto A^{D/2}$), transitions from $D \approx 1$ for small ponds to $D \approx 2$ for large ponds. The size (area) distribution of melt ponds has also been shown to be a power law [21]. Although several models reproduce these observations [22,23], a basic understanding of the reason for this behavior is lacking. In this Letter we will explain both of these observations using a simple geometric model without invoking any assumptions about the dynamics that govern the melt pond evolution.

Our model is a representation of post-drainage melt ponds. It consists of randomly placing circles of varying size on a plane and allowing them to overlap. The area

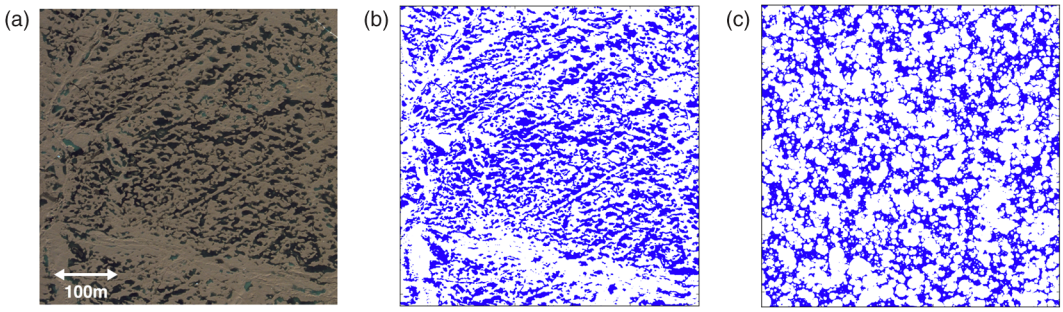

FIG. 1. (a) A photograph of melt ponds taken on August 7, 1998 during the SHEBA mission. (b) A binarized version of the same image. (c) A void model with a typical circle radius of $r_0 = 1.8$ m, and a coverage fraction of $\rho = 0.31$.

covered by circles in our model represents ice, while melt ponds are represented by the voids left between the circles [Fig. 1(c)]. Similar models are sometimes used to study transport properties in inhomogeneous materials, and are known as "Swiss cheese" models [24]. Physically, the circles can be thought of as regions where snow dunes used to be in the winter, and melt ponds fill in the space around them. Circle centers are placed with equal probability throughout the domain. Individual circles have radii r, randomly drawn from an exponential probability distribution $p(r) = (1/r_0)e^{-r/r_0}$, where r_0 is the mean circle radius and defines the physical scale for the model. We chose this probability distribution mainly due to its simple form, but all of our main conclusions are robust to using other distributions (see Supplemental Material [25], Sec. S4). After choosing r_0, the model is fully specified by choosing the fraction of the surface covered by voids ρ. To compare our model with melt pond data, we analyzed hundreds of photographs of sea ice taken during helicopter flights on multiple dates during the SHEBA mission of 1998 and the HOTRAX mission of 2005, and separated them into ice and pond categories using a machine learning algorithm [Figs. 1(a) and 1(b), Supplemental Material [25], Sec. S1]. In order to facilitate comparison with pond images, we implemented the void model on a grid with the same resolution and size as the pond images.

We begin the comparison by choosing the model parameters r_0 and ρ. To this end, we define two functions—the two-point correlation function $C(l)$ and a cluster correlation function $g(l)$, and compare them for pond images and the model. A two-point correlation function measures the probability that two points separated by a distance l are both located on *some* pond, while a cluster correlation function measures the probability that they are both located on the *same* pond. We first estimate r_0 using $C(l)$, because we can define it to be largely insensitive to changes in ρ (see below). Once we have calibrated r_0 by matching $C(l)$, we can choose ρ using $g(l)$.

For two points, $\mathbf{x}$ and $\mathbf{y}$, separated by a distance l, the two-point correlation function can be defined as

$$C(l) = \frac{\langle z(\mathbf{x})z(\mathbf{y})\rangle - \rho^2}{\rho(1-\rho)}, \tag{1}$$

where $z(\mathbf{x}) = 1$ if a point $\mathbf{x}$ is located on a pond, and $z(\mathbf{x}) = 0$ otherwise, and $\langle \ldots \rangle$ represents averaging over different points and over different images. Subtracting ρ^2 and dividing by $\rho(1-\rho)$ constrains $C(l)$ to vary between 1 and 0, and makes it insensitive to changes in ρ (see Supplemental Material [25], Sec. S2). The two-point correlation function determines a typical length scale of variability in melt pond coverage.

Plotting $C(l)$ for melt ponds on a semilog plot reveals that it is approximately a sum of two exponentials [Fig. 2(a)]. Therefore, there are two characteristic length scales in melt pond images—a small length scale comparable to the size of individual ponds and a large length scale that is comparable to the size of the image. The large length scale corresponds to variability of pond fraction due to large-scale ice features such as ridges or rafted ice floes. To focus on melt pond features, we have removed the contribution to $C(l)$ from large scale ice features by subtracting a fit to an exponential of $C(l)$ for $l > 25$ m. We varied this threshold, but found little difference in the results. After subtracting the fit, we normalized the remainder so that $C(0) = 1$ [inset of Fig. 2(a)]. We show the resulting functions for all of the available dates and compare them to the void model in Fig. 2(b). Ponds of all dates show similar $C(l)$ dropping by a factor of e after roughly 3.3 m. We found that this is well reproduced by the void model using $r_0 = 1.8$ m (see Supplemental Material [25], Sec. S2). The fact that the void model reproduces the shape of the two-point correlation function suggests that our assumption of randomly placing the circles is reasonable.

Next, we determine ρ. With this parameter, we wish to capture the pond geometric features such as the pond size distribution and the fractal dimension, rather than simply the pond coverage. For this reason, we do not set ρ equal to the pond coverage fraction of melt pond images, but instead we use the cluster correlation function to determine ρ. Essentially, the cluster correlation function $g(l)$ measures the probability that two points separated by a distance l belong to the same finite pond. However, there are some technical subtleties in how we define $g(l)$, and we give a precise definition in the Supplemental Material [25], Sec. S2.

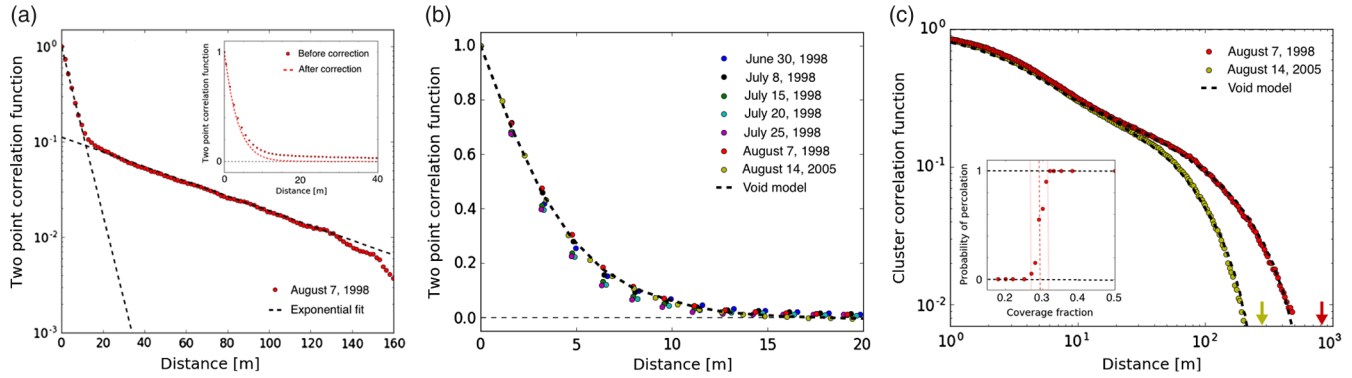

FIG. 2. (a) An example of the two-point correlation function $C(l)$ for melt ponds shown on a semilog plot. Dashed black lines represent fits to a small length scale exponential and a large length scale exponential. The inset shows $C(l)$ before and after a fit to the large length scale exponential has been subtracted. (b) A comparison between the two-point correlation function for ponds from 1998 and 2005 (circles), and the void model (dashed line). Ponds on all dates show a similar scale matched by the void model using $r_0 = 1.8$ m. (c) A comparison between the cluster correlation function $g(l)$ for August 7, 1998 (red circles), August 14, 2005 (yellow circles), and the void model using the same r_0 as in panel (b) (black dashed lines). Both model lines use $\rho = 0.31$, and the difference between them is due only to differing simulated image sizes. The image size for 1998 is indicated by a red arrow and the image size for 2005 is indicated by a yellow arrow. The fact that the exponential cutoff is set by the image size indicates that the ponds are roughly at the percolation threshold. The inset shows an independent estimation of the percolation threshold. Red points show the probability of finding a spanning cluster in the void model implemented on a grid the same size and resolution as the SHEBA images. The probability of finding a spanning cluster increases from 0 to 1 between $\rho = 0.28$ and $\rho = 0.31$.

In the model, in the limit of infinite domain size, there exists a well-defined coverage fraction ρ_c, the "percolation threshold," above which infinite clusters exist, and below which there is a maximum cluster size. The cluster correlation function in the void model sensitively depends on the deviation of the pond fraction from this percolation threshold, $|\rho - \rho_c|$ (see Supplemental Material [25], Sec. S2). Below and above the percolation threshold, the cluster correlation function is greater than zero up to a certain distance, after which it exponentially decreases. As the coverage fraction approaches the percolation threshold, this cutoff length grows, and sufficiently close to the threshold it is set by the image size. The location of the exponential cutoff quantifies the typical size of the largest finite connected pond cluster. We discuss the functional form of $g(l)$ in detail in the Supplemental Material [25], Sec. S6.

Narrow connections between ponds are often missed by the image processing algorithm so that for many dates $g(l)$ depends on the artificial threshold parameter used in the machine learning algorithm to separate ice from ponds (see Supplemental Material [25], Sec. S1, for details). The only dates after pond drainage for which $g(l)$ is stable against changes in this threshold are August 7 of 1998 and August 14 of 2005. In Fig. 2(c), we compare the cluster correlation function for the void model and data on those dates. Remarkably, the pond clusters for both dates appear to be organized very near the percolation threshold, as indicated by the fact that the length scale of exponential cutoff in $g(l)$ is set by the image size. In Fig. 2(c) we use $\rho = 0.31$ to match the pond data, and the difference between $g(l)$ for the ponds from 1998 and ponds from 2005 is solely due to a different image size. In fact, using any ρ from a range $0.28 < \rho < 0.31$ provides an equally good fit to the data, which indicates that within this entire range the size of the largest pond is determined by the image size. To independently confirm that ponds are well described by the void model near the percolation threshold, we ran the void model, 50 times at multiple values of ρ, and found the probability of forming a cluster that spans at least one dimension of the image [inset of Fig. 2(c)]. We found that this probability increases from 0 to 1 between $\rho = 0.28$ and $\rho = 0.31$, which closely matches the range of coverage fractions that fit the pond $g(l)$. We note that although we chose ρ to match the cluster structure between the model and the data, the value we found agrees reasonably well with the pond coverage fraction on those dates ($30\% \pm 5\%$ on August 7 of 1998, and around $40\% \pm 5\%$ on August 14 of 2005). We discuss the relationship between the pond coverage fraction and pond geometry in detail in the Supplemental Material [25], Sec. S6.

It is remarkable that the properties of ponds from 1998 and 2005, which likely developed under very different environmental conditions, are so similar: the correlation functions for both years are well fit by the void model using the same r_0 and ρ. This is particularly surprising since sea ice during the 1998 mission had a large proportion of multiyear ice, whereas ice during the 2005 mission was predominantly first-year ice.

Having chosen r_0 and ρ, we can proceed to explain the observations of pond fractal dimension and size distribution. Following Hohenegger *et al.* [20], we define the fractal dimension of the pond boundary as the exponent that relates the area and the perimeter of the pond, $P \propto A^{D/2}$.

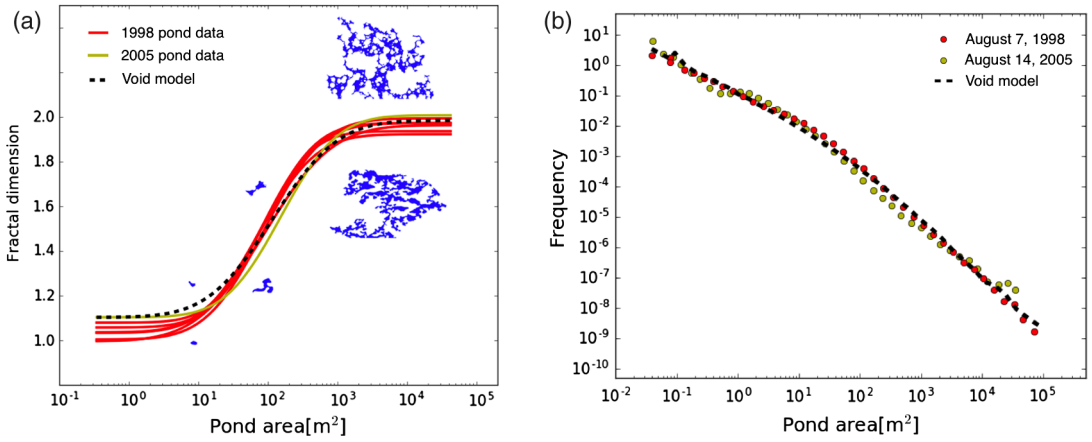

FIG. 3. (a) A comparison between the fractal dimension of pond boundaries for different dates after pond drainage from 1998 (red curves), 2005 (yellow curve), and the void model with r_0 and ρ the same as in Fig 2 (black dashed curve). Examples of ponds (below the curve) and voids (above the curve) of various sizes are also shown. (b) Size distribution for ponds on August 7, 1998 (red dots), ponds on August 14, 2005 (yellow dots), and the void model (black dashed line).

The fractal dimension can vary between the fundamental limits of $D = 1$ for regular shapes such as circles to $D = 2$ for space filling or linear shapes. We find D as a function of A by fitting a curve to the area-perimeter data. We explain the details of this fitting procedure in the Supplemental Material [25], Sec. S3.

In Fig. 3(a) we find D as a function of A for pond data on all dates from the summer of 1998 after pond drainage (red curves) and 2005 (yellow curve). Our results are consistent with Hohenegger *et al.* [20], with the pond fractal dimension transitioning from $D \approx 1$ to $D \approx 2$ at $A_c \approx 100$ m^2, and a transition range spanning roughly 2 orders of magnitude. Without any tuning other than choosing r_0 and ρ using the correlation functions, the void model is able to match the observed transition in pond fractal dimension nearly perfectly [Fig. 3(a), black dashed curve].

In the Supplemental Material [25], Sec. S7, we give an argument that a transition from $D < 2$ to $D \approx 2$ is a generic consequence of individual objects connecting and, therefore, cannot be used as strong support for any particular physical model of melt ponds. On the other hand, matching the fractal transition scale and the transition range are nontrivial, and cannot be reproduced by an arbitrary model of randomly connecting objects (see Supplemental Material [25], Sec. S9). At small sizes, the void model predicts a dimension slightly larger than 1, likely corresponding to the fact that small voids are not necessarily simple smooth shapes. It is possible that small-scale physical processes in real ponds, such as erosion of pond walls, are responsible for smoothing small ponds into more circular shapes with $D \approx 1$.

Finally, we compare the pond size distribution with the void model in Fig. 3(b). Again as a result of sensitivity to the threshold parameter in the machine learning algorithm, we only use pond data for August 7th of 1998 and August 14th of 2005. At scales larger than roughly 10 m^2 the pond size distribution follows an approximate power law, in agreement with previous findings. The power law behavior is particularly clear for ponds from 1998, and the power law exponent (approximately 1.8) is slightly larger than previously found [21]. Using the same r_0 and ρ as before, the void model reproduces the pond size distribution over the entire range of observations, more than 6 orders of magnitude. This matching is highly robust: the void model matches the pond size distribution even at the smallest scales regardless of details such as the circle radius distribution or the shape of the objects placed randomly (see Supplemental Material [25], Sec. S4).

We have shown that a simple model of voids surrounding overlapping circles captures key geometric patterns of Arctic melt ponds with high fidelity and robustness, with only two parameters that can be chosen naturally by comparing the model and the data. Our model is purely geometric, and can therefore be used as a benchmark against which to test any physical model. This work shows that much of melt pond geometry can be understood simply by assuming that melt ponds are placed randomly and have a typical size. Even though many models will reproduce the same universal features, our model is special in that it captures quantitative details of melt pond geometry beyond what an arbitrary model of connecting objects is capable of doing. Our work raises two critical questions about melt pond physics that must be answered. First, why does the pond scale appear to be so robust for ponds evolving under differing environmental conditions, and, second, why do ponds seem to be organized near the percolation threshold? The answer to the second question may be particularly interesting, as it may point to self-organized critical behavior in melt ponds, and may suggest that the pond coverage fraction is more constrained than previously thought. Answering these questions may yield deeper insight into melt pond physics

and allow for a better representation of this important process in global climate models.

We thank Don Perovich for providing the image data. We thank Djordje Spasojević and Alberto Petri for discussions about correlation functions and the percolation threshold. We thank Douglas MacAyeal for reading the Letter and giving comments. We thank three anonymous reviewers for constructive comments. P. P. was supported by a NASA Earth and Space Science Fellowship. B. B. C. was supported by the National Science Foundation Graduate Research Fellowship Program, Grant No. 2388357. This work was partially supported by the National Science Foundation under NSF Grant No. 1623064.

*To whom all correspondence should be addressed.
ppopovic@uchicago.edu

[1] D. K. Perovich and J. A. Richter-Menge, Loss of sea ice in the arctic, Annu. Rev. Mar. Sci. **1**, 417 (2009).
[2] J. M. Grebmeier, W. O. Smith, and R. J. Conover, Biological processes on Arctic continental shelves: Ice-ocean-biotic interactions, in *Coastal and Estuarine Studies* (American Geophysical Union, Washington, DC, 1995), pp. 231–261.
[3] M. C. Serreze, M. M. Holland, and J. Stroeve, Perspectives on the arctic's shrinking sea-ice cover, Science **315**, 1533 (2007).
[4] J. Stroeve, M. M. Holland, W. Meier, T. Scambos, and M. Serreze, Arctic sea ice decline: Faster than forecast, Geophys. Res. Lett. **34**, L09501 (2007).
[5] M. M. Holland and J. A. Curry, The role of physical processes in determining the interdecadal variability of central Arctic sea ice, J. Clim. **12**, 3319 (1999).
[6] M. M. Holland, D. A. Bailey, B. P. Briegleb, B. Light, and E. Hunke, Improved sea ice shortwave radiation physics in ccsm4: the impact of melt ponds and aerosols on Arctic sea ice, J. Clim. **25**, 1413 (2012).
[7] D. K. Perovich, Cold Regions Research and Engineering Lab Technical Report No. ADA310586 1996.
[8] M. Morassutti and E. LeDrew, Albedo and depth of melt ponds on sea-ice, International Journal of Climatology **16**, 817 (1996).
[9] D. Schröder, D. L. Feltham, D. Flocco, and M. Tsamados, September Arctic sea-ice minimum predicted by spring melt-pond fraction, Nat. Climate Change **4**, 353 (2014).
[10] M. Lüthje, D. Feltham, P. Taylor, and M. Worster, Modeling the summertime evolution of sea-ice melt ponds, J. Geophys. Res. C **111**, C02001 (2006).
[11] P. Taylor and D. Feltham, A model of melt pond evolution on sea ice, J. Geophys. Res. C **109**, C12007 (2004).
[12] D. Flocco and D. L. Feltham, A continuum model of melt pond evolution on Arctic sea ice, J. Geophys. Res. C **112**, C08016 (2007).
[13] E. D. Skyllingstad, C. A. Paulson, and D. K. Perovich, Simulation of melt pond evolution on level ice, J. Geophys. Res. C **114**, C12019 (2009).
[14] C. Polashenski, D. Perovich, and Z. Courville, The mechanisms of sea ice melt pond formation and evolution, J. Geophys. Res. C **117**, C01001 (2012).
[15] J. Landy, J. Ehn, M. Shields, and D. Barber, Surface and melt pond evolution on landfast first-year sea ice in the Canadian Arctic Archipelago, J. Geophys. Res. C **119**, 3054 (2014).
[16] C. Petrich, H. Eicken, C. M. Polashenski, M. Sturm, J. P. Harbeck, D. K. Perovich, and D. C. Finnegan, Snow dunes: A controlling factor of melt pond distribution on Arctic sea ice, J. Geophys. Res. C **117**, C09029 (2012).
[17] E. D. Skyllingstad and C. A. Paulson, A numerical study of melt ponds, J. Geophys. Res. C **112**, C08015 (2007).
[18] A. E. Arntsen, A. J. Song, D. K. Perovich, and J. A. Richter-Menge, Observations of the summer breakup of an Arctic sea ice cover, Geophys. Res. Lett. **42**, 8057 (2015).
[19] K. E. Frey, D. K. Perovich, and B. Light, The spatial distribution of solar radiation under a melting Arctic sea ice cover, Geophys. Res. Lett. **38**, L22501 (2011).
[20] C. Hohenegger, B. Alali, K. Steffen, D. Perovich, and K. Golden, Transition in the fractal geometry of Arctic melt ponds, The Cryosphere **6**, 1157 (2012).
[21] D. Perovich, W. Tucker, and K. Ligett, Aerial observations of the evolution of ice surface conditions during summer, J. Geophys. Res. C **107**, 8048 (2002).
[22] B. Bowen, C. Strong, and K. M. Golden, Modeling the fractal geometry of Arctic melt ponds using the level sets of random surfaces, J. Fractal Geom. (to be published).
[23] Y.-P. Ma, I. Sudakov, and K. M. Golden, Ising model for melt ponds on Arctic sea ice, arXiv:1408.2487.
[24] B. I. Halperin, S. Feng, and P. N. Sen, Differences between Lattice and Continuum Percolation Transport Exponents, Phys. Rev. Lett. **54**, 2391 (1985).
[25] See Supplemental Material at http://link.aps.org/supplemental/10.1103/PhysRevLett.120.148701 for a discussion of image processing, correlation functions, fractal dimension, robustness and limitations of the model, the relationship between pond coverage and geometry, the reason for the fractal transition, an analysis of ponds before drainage, and alternative models of pond geometry. The Supplemental Material includes Refs. [22,23,26–32].
[26] B. Mandelbrot, How long is the coast of britain? Statistical self-similarity and fractional dimension, Science **156**, 636 (1967).
[27] A. Aharony and D. Stauffer, *Introduction to Percolation Theory* (Taylor & Francis, New York, 2003).
[28] J. W. Essam, Percolation theory, Rep. Prog. Phys. **43**, 833 (1980).
[29] N. Goldenfeld, *Lectures on Phase Transitions and the Renormalization Group* (Addison-Wesley, Advanced Book Program, Reading, MA, 1992).
[30] G. Delfino, J. Viti, and J. Cardy, Universal amplitude ratios of two-dimensional percolation from field theory, J. Phys. A **43**, 152001 (2010).
[31] A. R. Kerstein, Equivalence of the void percolation problem for overlapping spheres and a network problem, J. Phys. A **16**, 3071 (1983).
[32] A. Sicilia, J. J. Arenzon, A. J. Bray, and L. F. Cugliandolo, Domain growth morphology in curvature-driven two-dimensional coarsening, Phys. Rev. E **76**, 061116 (2007).